The Neftegorsk (Sakhalin Island) 1995 earthquake: a rare interplate event

S. Arefiev, E. Rogozhin, R. Tatevossian, Luis Rivera, A. Cisternas

Geophys. J. Int. (2000) **143,** 595–607

The Neftegorsk (Sakhalin Island) 1995 earthquake: a rare interplate event

S. Arefiev,[1] E. Rogozhin,[1] R. Tatevossian,[1] L. Rivera[2] and A. Cisternas[2]

[1] *Institute of Physics of the Earth, Russian Academy of Sciences,* 123810 *Moscow, B. Gruzinskaya* 10, *Russia. E-mail: arefiev@synapse.ru*
[2] *Institut de Physique du Globe,* 5 *rue René Descartes,* 67084 *Strasbourg, France. E-mail: armando@sismo.u-strasbg.fr*

Accepted 2000 May 24. Received 2000 May 22; in original form 1999 October 29

SUMMARY

The Neftegorsk 1995 May 27 earthquake ($M_S = 7.6$) occurred in the northern part of Sakhalin Island in a region considered to be a fairly inactive plate boundary between the North American and Eurasian plates. Coseismic surface ruptures are associated with the Upper Piltoun fault, a secondary feature joining the Sakhalin–Hokkaido and Middle Sakhalin faults, which are the main tectonic elements of the region. Observations obtained during a field experiment that included a local seismic network, neotectonics and geodetic measurements are combined with the analysis of satellite images and a broad-band body wave inversion. A complex source model consisting of four branches is proposed. The two main branches, oriented N–S, show right-lateral strike-slip motion. The rupture nucleates between these two segments and propagates bilaterally. We estimate a total rupture length of 46 km, a width of 12 km, and an average slip value of 3.9 m. However, the maximum observed value of surface slip is 8.1 m, an unusually large value for an event of this magnitude. This earthquake supports the model of a North American plate rotating clockwise with respect to Eurasia.

Key words: aftershocks, body waves, earthquakes, inversion, plate boundaries, surface rupture.

INTRODUCTION

The Neftegorsk 1995 May 27 earthquake ($M_S = 7.6$ by NEIC and Obninsk) occurred in the northern part of Sakhalin Island in eastern Russia. It was the most destructive earthquake within the present territory of Russia (all previous large earthquakes in the former Soviet Union, for example Ashkhabad 1948, Spitak 1988, took place within the territory of the newly independent countries). About 2000 people were killed. This earthquake is of great interest not only because of its catastrophic consequences, but also because of its geographical position—the rupture is located along a plate boundary that is not well characterized. The epicentre is located about 1000 km from the NUVEL-1A pole for the motion of North America relative to Eurasia. Thus, the kinematics of the source of the Neftegorsk earthquake gives important new data for understanding and constraining the details of the plate motions there. The geology and tectonics of the region are not well known, since the surface is mostly covered by young sediments, and basement rocks are not exposed. Moreover, no earthquake of such large magnitude had ever been reported at the site of the Neftegorsk earthquake, and the event was totally unexpected. The General Seismic Zoning map published in the USSR in 1978, an official document, did not include any event with magnitude $M > 6$ in this part of Sakhalin Island.

An expedition organized by the Institute of Physics of the Earth (Moscow), the Institute of Marine Geology and Geophysics (Yuzhno-Sakhalinsk), both part of the Russian Academy of Sciences, and by the Research Centre for Earthquake Prediction, Hokkaido University, Japan studied the Neftegorsk earthquake in the field. Preliminary results were published in The Neftegorsk earthquake of 27(28).05.1995 (1995).

In this paper we study and analyse the results of field observations from the expedition, satellite images, and broad-band seismograms from the global network for the main shock. We model the geometry and the time history of the main rupture and propose an interpretation for it.

As a first approximation, the main shock can be described as a simple shock by the best double-couple of the Harvard CMT solution. This mechanism fits well with the observed main surface rupture. The moment tensor has, however, a significant non-double-couple component (15 per cent), a phenomenon that is not uncommon but that implies a more complex character for the event. Details of the cluster geometry of aftershocks, branching of the surface ruptures, features of the satellite images (structures oriented perpendicular to the main rupture), and the waveforms allow us to reconstruct a more realistic and detailed source model for the Neftegorsk earthquake.

TECTONIC SETTING AND SEISMIC HISTORY

The position of the earthquake is shown in Fig. 1(a), with the location of the pole of rotation of the Eurasian plate with respect to the North American plate shown by a solid diamond (DeMets *et al*. 1990). The relative motion of the plates is roughly consistent with the mechanism of the source (the Harvard solution is plotted in Fig. 1b). More details of the tectonic setting (north Sakhalin) can be seen in Fig. 1(c), which is simplified from Rogozhin (1996) and includes information from Kharakhinov *et al*. (1984), Semenov *et al*. (1996) and Rozhdestvenskiy (1975). The main structure here is the N–S-oriented Sakhalin–Hokkaido right-lateral strike-slip fault, running along the eastern side of the island and moving at a rate of about 4 mm yr^{-1} if we use either NUVEL-1 or NUVEL-1A plate motions (an independent measure made at Schmidt peninsula, north of Sakhalin gives 14 km offset of Pliocene units in 4 million years). Its length is at least about 1000 km from north to south. Some secondary faults join it, one of which is the Upper Piltoun fault oriented NNE–SSW (number 3 in Fig. 1c).

The seismicity of the region is plotted in Fig. 2, using data from the Russian (ex-Soviet) seismic network. Some artefacts in the form of horizontal and vertical lines were generated by the round-off of epicentral coordinates in the catalogue. We added a small random error to the coordinates (5 km standard deviation) in order to reduce such a strong visual effect. The network of stations was never dense in the region, and, furthermore, it has been greatly reduced in recent years, negatively affecting the quality of the catalogue. Moreover, the period of seismic history is short. There are no ancient historical data,

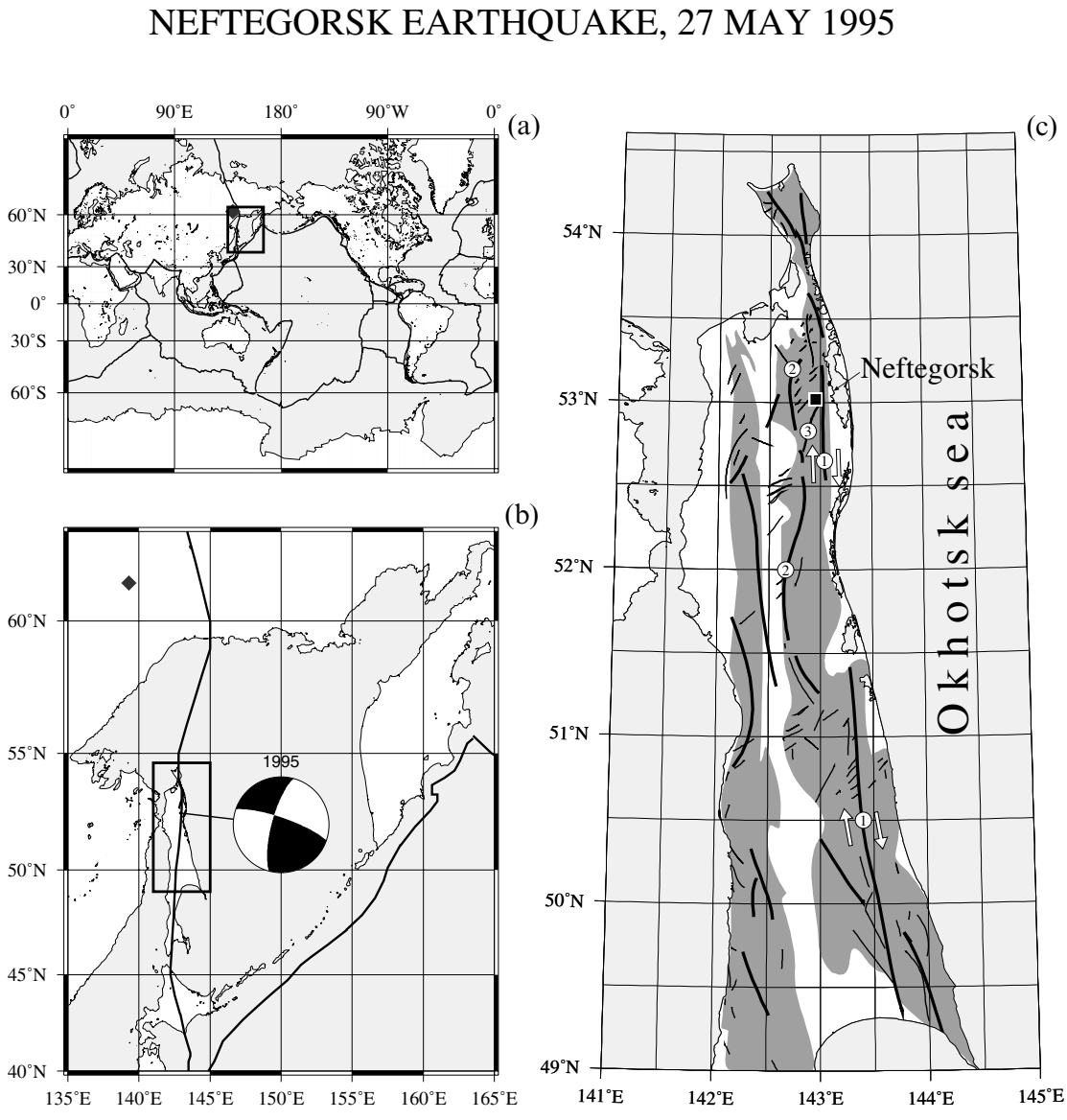

Figure 1. Location of the Neftegorsk earthquake: (a) on the world map of plate tectonics; (b) on a regional scale together with the Harvard CMT solution. Filled diamond symbols indicate the NUVEL-1A pole of rotation of North America with respect to Eurasia. (c) Main faults of the northern part of Sakhalin Island: (1) Sakhalin–Hokkaido fault; (2) Middle Sakhalin fault; (3) Upper Piltoun fault. Shaded areas are orogenic uplifts. Arrows show the fault slip direction.

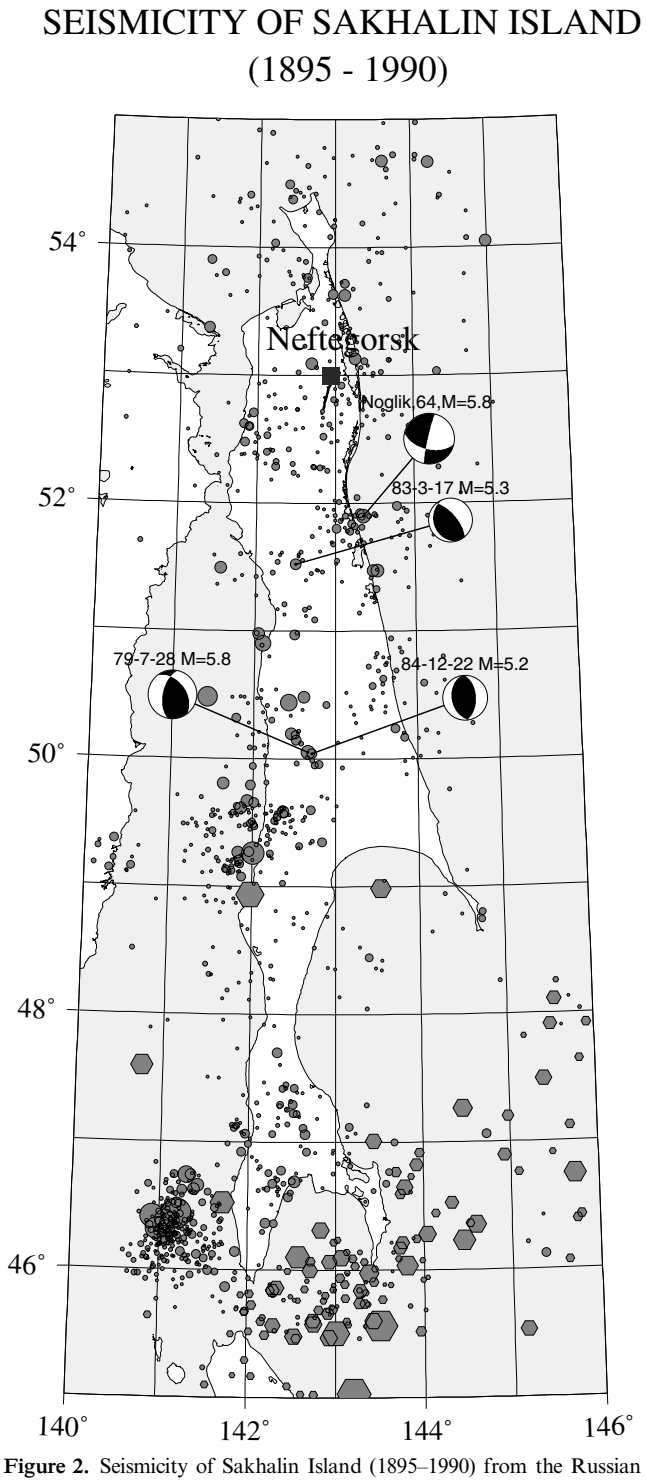

Figure 2. Seismicity of Sakhalin Island (1895–1990) from the Russian Seismic Network. Magnitudes vary between 3.3 and 7.5. The best double-couple mechanisms of available Harvard CMT solutions previous to the Neftegorsk earthquake, and the mechanism of the 1964 Noglik earthquake are shown. The hexagons show deep seismicity related to the Kuril–Kamchatka arc.

simply because of the absence of permanent populations and towns, even in the recent past. The catalogue of historical earthquakes starts in 1895, at practically the same time as the beginning of worldwide instrumental observations.

Both shallow and deep (300 km and more) earthquakes occur under Sakhalin. Deep earthquakes are represented by hexagons in Fig. 2. Most deep events are located south of Sakhalin, and are associated with the Kuril–Kamchatka subduction zone, which dips from east to west, and is one of the most seismically active regions in the world. Shallow seismicity does not display any clear structural pattern. The cluster to the southwest of the Island is related to the strongest shallow event observed before the Neftegorsk earthquake in this region—the Moneron earthquake (1970 September 5, 142°.9E, 46°.4N, $M_S = 7.5$) and its aftershocks.

Fig. 2 also shows the only four source mechanisms for shallow events obtained before 1995. There are three Harvard CMT solutions, indicating the relatively low level of seismic activity in the region during the past 20 years. The fourth one corresponds to the Noglik, 1964 October 2 earthquake, $M_S = 5.8$ (Oskorbin *et al.* 1967), and was obtained before the era of Harvard CMT solutions. The Noglik earthquake is the strongest known earthquake in northern Sakhalin Island prior to the Neftegorsk earthquake. Its mechanism corresponds to right-lateral strike-slip, with some amount of dip-slip, along the Sakhalin–Hokkaido fault. It is clear that, even if the weaker events have thrust mechanisms, the strongest ones (the Neftegorsk and Noglik earthquakes) show predominantly strike-slip motion. In addition, the Noglik and the Neftegorsk earthquakes are related to different faults.

MAIN TECTONIC FEATURES FROM DIGITAL ELEVATION MODELS AND SATELLITE IMAGES

The tectonic structures of the Neftegorsk earthquake region are shown in Figs 3(a) and (b). We present there the main features, faults and folds, from the analysis of digital elevation models (30′ grid size from GTOPO30, USGS, EROS Data Center) (Fig. 3a), and the interpretation of the satellite images prepared by the Russian State Center 'Nature' in 1982 from data obtained in 1980 (Fig. 3b). We also show, by a large arrow, the direction of the relative motion between the Eurasian and the North American plates. The direction of the main compressional stress σ_1 matches the direction of relative convergence closely, it is orthogonal to the orientation of folding, and makes an angle of about 45° with the N–S-oriented strike-slip dextral faulting.

The main fault in the region is the N–S-oriented Sakhalin–Hokkaido right-lateral strike-slip system ('1' in Fig. 3), which can be seen along the eastern side of the island. It consists of a series of short breaks of similar orientation. Another important feature is the Middle Sakhalin fault ('2' in Fig. 3), which is oriented roughly N–S and exhibits a dominant right-lateral strike-slip character, but which shows a much more complex structure than the Sakhalin–Hokkaido fault. In fact, it consists of several segments and branches. The surface ruptures activated during the Neftegorsk earthquake correspond to the Upper Piltoun mainly right-lateral strike-slip fault ('3' in Fig. 3), which is oriented NNE and connects the Sakhalin–Hokkaido and the Middle Sakhalin faults. The Upper Piltoun fault is about 40 km long and its trace was visible before the earthquake.

The Middle Sakhalin fault ('2' in Fig. 3) shows a left step at a latitude of about 52.8°. South of this step there is a push-up basin, limited to the north and south by reverse faulting. The N–S-oriented segment south of the step exhibits a series of en échelon folds oriented perpendicular to the relative plate

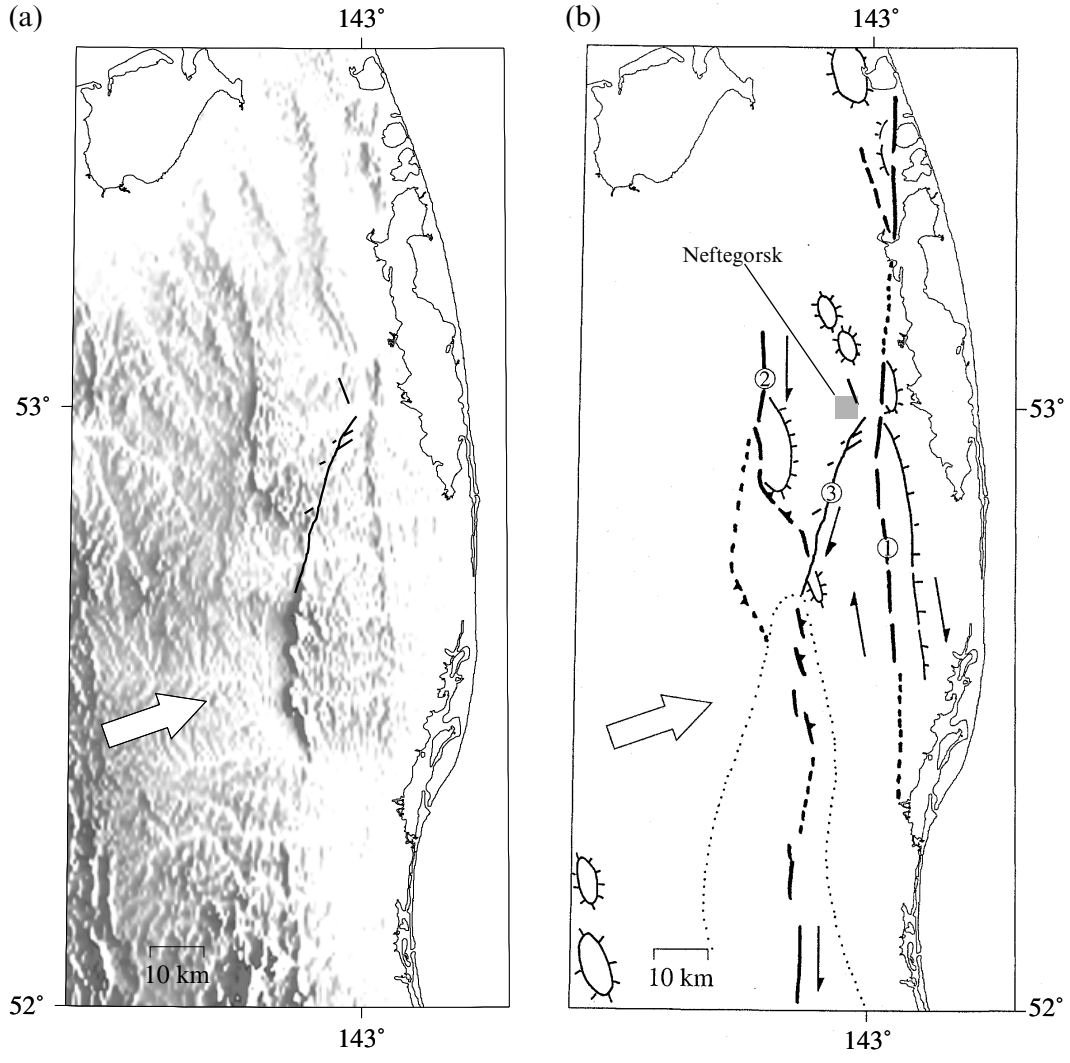

Figure 3. (a) Digital elevation model of the Neftegorsk region from Photoplan, Priroda, scale 1/1000 000, 1982. The white thick arrow indicates the relative motion (NUVEL-1A) of North America with respect to Eurasia. Black lines indicate the 1995 surface ruptures. (b) Main faults (thick lines): (1) Sakhalin-Hokkaido; (2) Middle Sakhalin; and (3) Upper Piltoun. Thin arrows show the dextral sense of motion. Anticlines are shown by closed or half-open thin lines with tick marks separating Miocene (inside) from Pliocene sediments. A large-scale anticline is shown by the dotted line.

motion and to the main compressional direction. The N–S-oriented Sakhalin–Hokkaido fault ('1' in Fig. 3) also shows a bifurcation near a latitude of 53°. The bifurcation region coincides with a change of direction of the Neftegorsk surface ruptures, with the southern end of the aftershock cluster located north of the city of Neftegorsk (Figs 5 and 6), and with a minimum of the measured dislocation (Fig. 4). Another aftershock cluster at 53°N and 20 km west of the surface ruptures (Fig. 5) coincides with another bifurcation of the Middle Sakhalin fault ('2' in Fig. 3).

The main faults are related in most places to linear ridges oriented N–S. The N–S orientation of the topography is cut by several E–W-oriented valleys and rivers. Several of these rivers are offset in a right-lateral sense by the Middle Sakhalin fault.

Folding is present at several scales, and affects mainly Miocene and Pliocene sediments, indicating rather young deformation and shortening in this region. Most of the axes of folding are perpendicular to the main direction of compression and of plate convergence. The topography also shows the effect of differential erosion of the folded layers.

SURFACE RUPTURE

Surface ruptures were studied in detail by an international team working in the epicentral region (Rogozhin 1995, 1996). The sites of neotectonic observations were accurately located by portable GPS receivers. Most of the work was carried out by Kozhurin & Streltsov (1995), who visited practically all of the ruptures, measuring displacements directly across the fault. The northern part of the fault was also investigated in detail by members of a Japanese expedition. Other specialists working along some sectors of the surface breaks always refer to Kozhurin & Streltsov (1995), but give a slightly different account of the shape of the fault trace and of the vertical and horizontal displacement (Ivashenko *et al.* 1995; Kozhurin & Streltsov 1995; Shimamoto *et al.* 1995a; Rogozhin 1995, 1996). The most complete mapping of the surface fault, including secondary ruptures, is that by Rogozhin (1995, 1996).

We present here a synthesis of the data contained in previous publications, including the original readings of Kozhurin (more than 50 points of measurement), in order to construct a surface

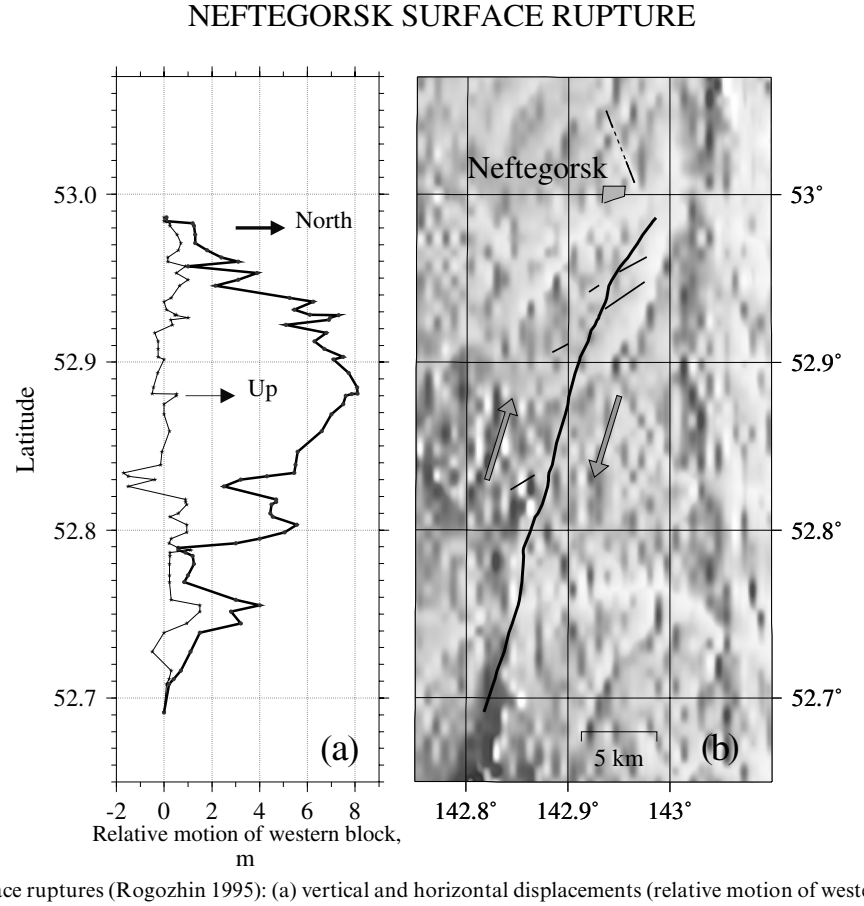

Figure 4. Coseismic surface ruptures (Rogozhin 1995): (a) vertical and horizontal displacements (relative motion of western block) in metres along the main fault as a function of latitude. (b) Map of the scarps—topography from Photoplan, Priroda, scale 1/1000 000 1982.

rupture map with precise observations of horizontal and vertical displacements. The rupture reaches 46 km in length, if we include the branch north of the city of Neftegorsk which is described by Rogozhin (1995) as having a strike of N160° and a length of 6 km. However, the length of the main rupture is only 35 km. The dip of the fault is 60°–70° towards the west (according Rogozhin 1995 and to the depth distribution of aftershocks), but it becomes almost vertical near the surface (according to Shimamoto *et al.* 1995a). Fig. 4 shows the map of the fault trace, and a graph of vertical and horizontal displacements along the fault.

Using this figure we estimated that the average lateral displacement along the surface is 3.9 m. Horizontal displacement is dominant all along. The amplitude of the lateral offset as a function of distance along the fault shows three main arcs (with endpoints at 52.7°N, 52.79°N, 52.83°N and 52.98°N in Fig. 4a), suggesting three segments. The maximum right-lateral dislocation reaches 8.1 m on the northern segment, at 52.88°N (Shimamoto *et al.* 1995a, b). The southern end of the second segment (at 52.79°N) coincides with a change in orientation of the fault trace.

The maximum vertical displacement reaches 1.7 m. Most of the western block has been uplifted, but there is a significant downthrow around 52.83°N.

The secondary branches of the surface rupture are of discontinuous character, in contrast to the continuity of the main surface rupture.

AFTERSHOCKS

A temporary seismic network of 12 stations (six three-component analogue short-period telemetric stations and six three-component short-period digital autonomous stations) was installed in the epicentral region from 1995 June 10 to July 7. A catalogue of recorded aftershocks includes about 700 events (Arefiev *et al.* 1995). Epicentres and depths were calculated using the HYPO71 routine (Lee & Lahr 1975), but only one-third of the aftershocks were assigned a magnitude. The velocity model is given in Table 1(a). We calculated the local magnitude of the remaining aftershocks from the Russian definition of energy class K ($K = 1.8$ Mag $+ 4$), using the absolute value of the amplitude of P and S waves at several stations and taking the average of individual magnitudes.

The map of recorded aftershocks (only events with an epicentral location error of less than 5 km were included) is shown in Fig. 5, together with the location of the temporary seismic stations and the observed surface ruptures. The north-eastern region is covered better by the seismic network than the southwestern one. Field conditions in the epicentral region, and difficulty of access to the southern part, limited the geometry of the portable network.

The main surface rupture trends NNE, and most of the aftershock activity is concentrated west of it, indicating westward dip. A cluster in the northeastern part of the zone correlates well with the northern end of the surface rupture, which is a

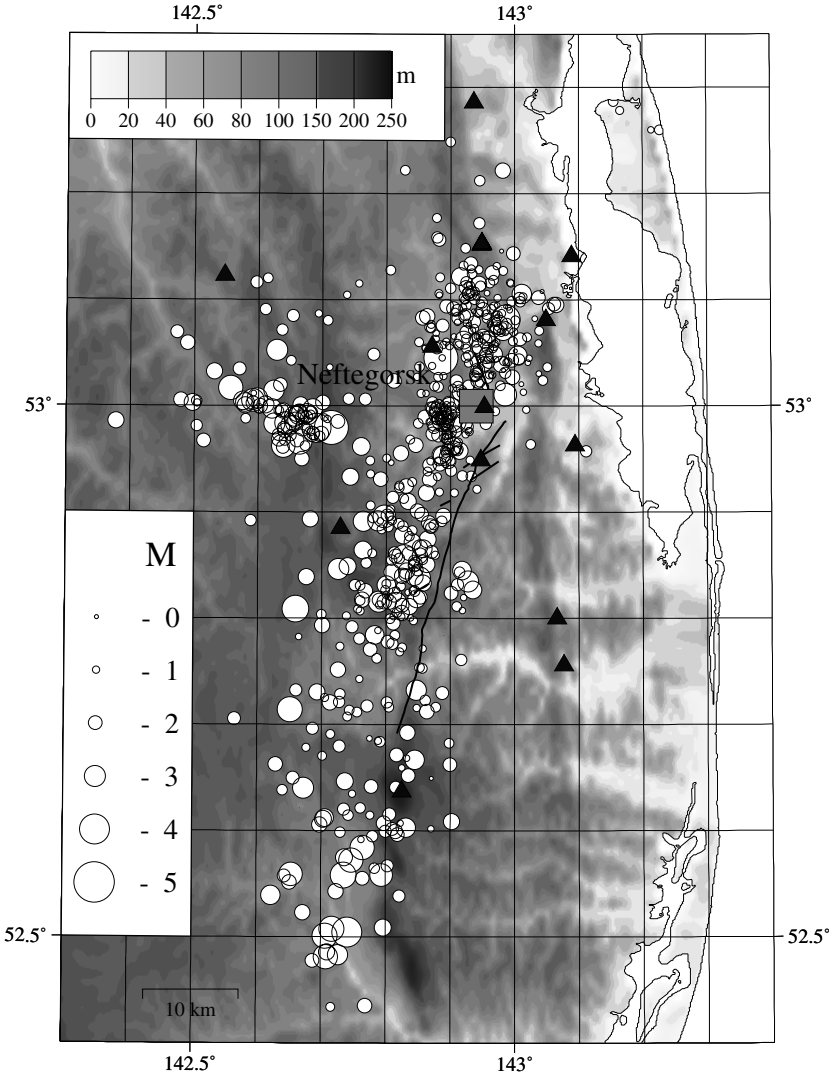

Figure 5. Circles show the epicentres of the 539 best quality aftershocks (error <5 km) from 1995 June 10 to July 7. Triangles show the temporary seismic network. The square is the city of Neftegorsk.

Table 1(a). Velocity model for Hypo71. Z_{top} is the depth of the top of the layer.

Layer	Z_{top} (km)	V_P (km s^{-1})
1	0	4.0
2	5	5.6
3	15	6.4
4	33	7.75

Table 1(b). Simplified velocity model.

Layer	Z_{top} (km)	V_P (km s^{-1})	V_S (km s^{-1})	Poisson's ratio
1	0	4.0	2.3	2.6
2	5	6.4	5.7	2.8

segment oriented NW–SE. The geometry of the surface ruptures suggests that this northernmost branch is a thrust fault, which is compatible with the dextral character of the main fault. Another cluster oriented roughly NW–SE, and including important aftershocks, can be recognized at (142.6°E, 53°N), but no surface ruptures were found on top of it. We cannot be certain whether this cluster appeared later, as the result of a strong aftershock, or if it originated during the main shock, since we started recording two weeks after the earthquake. We will see below that the second possibility is more reasonable.

We used only the more accurate locations (average depth error about 2–3 km) in order to study the depth distribution of aftershocks. The corresponding map of epicentres, cross-sections, and one histogram showing the distribution of aftershocks by depth, are given in Fig. 6. The frequency distribution of aftershock depths has a maximum at roughly 10 km, and few of the events show depths greater than 15 km. This leads to an estimation of 15 km for the maximum depth of the main brittle rupture (cross-section A). We should mention that the local peaks of the histogram of aftershocks at a depth of 4 km might be due to the velocity model of Table 1(a). Cross-section A also suggests a concentration of aftershocks around the areas broken by the main shock. We can see at least two

DEPTH DISTRIBUTION OF AFTERSHOCKS

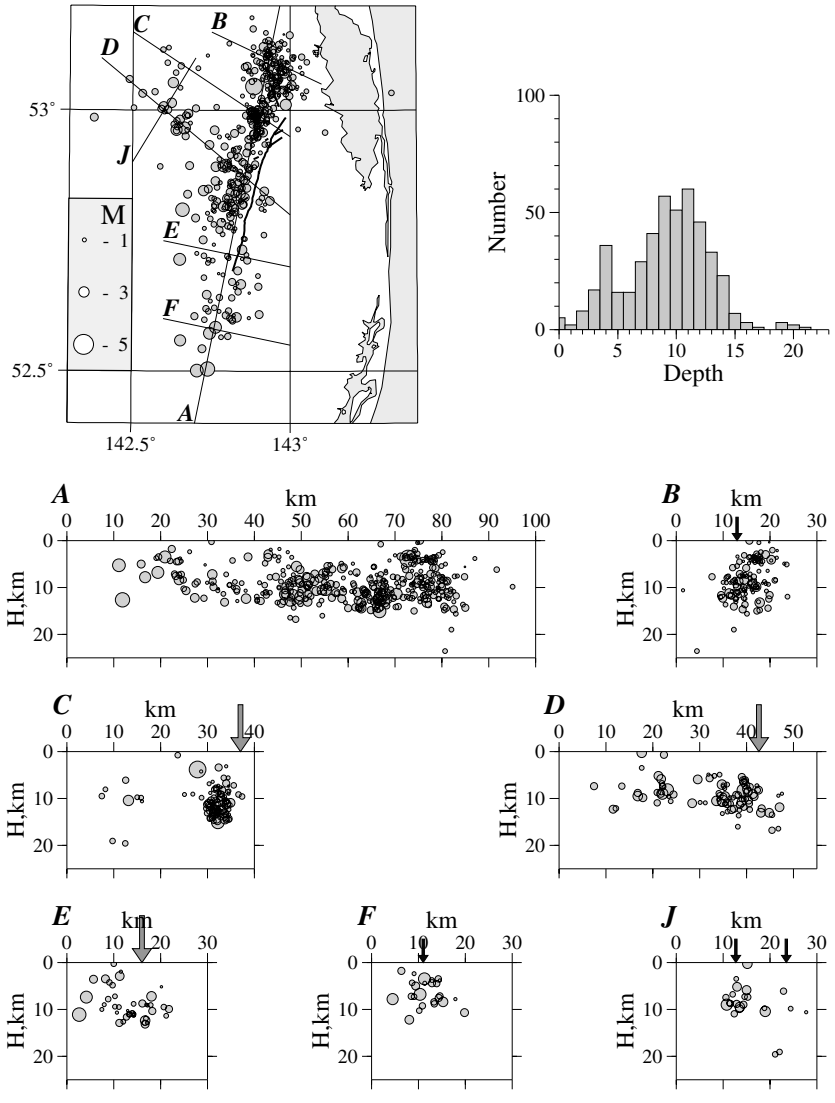

Figure 6. Map of epicentres of accurately located aftershocks, and cross-sections A to J. Magnitudes vary between 0.6 and 5.0. The histogram shows the depth distribution of all aftershocks. Cross-section A is longitudinal along the main rupture. The maximum depth is about 15 km. Horizontal distances are in kilometres. The large vertical arrows indicate the position of the main surface rupture. Smaller arrows indicate the locations of transverse cross-sections.

broken segments of different size (20–45 km, and 45–75 km) surrounded by aftershocks (Fig. 4). The linear alignment of aftershocks west of the fault, and cross-section C suggest a 70° westward dip of the main fault. This value is consistent with the observations in a trench across the fault giving a westward dip of 60° (Rogozhin 1995), and with the CMT focal mechanism given by Harvard. Cross-sections D and J show the maximum and minimum extension of the western aftershock cloud passing through their intersection. Thus, this cloud is oriented NW, rather than being parallel to the main rupture. Finally, cross-section E confirms that most aftershocks are west of the fault trace.

There were five focal mechanisms determined by Harvard. The locations of two of them (recorded on June 13) were determined with greater accuracy since the epicentral network was working at that time. The map of the strongest aftershocks obtained by the local network, and the CMT solutions with the NEIC locations are plotted in Fig. 7. It is possible to observe the shift of the NEIC determinations (small open circles) with respect to the ones that are well controlled by the local network (filled circles). The NEIC epicentre for the main shock was located near the southern end of the surface breaks and the depth was fixed at 33 km, suggesting northward rupture propagation. The first shock of June 13 (June 13a) is located near the NW-oriented segment north of the surface rupture, and the orientation of one of its nodal planes (NW) is very well correlated to it, the dip being 50° to the NE, corresponding to a thrust with a left-lateral component. This mechanism is consistent with the interpretation of motion along faults of similar orientation (Fig. 3). The second event on June 13 (June 13b), almost a pure thrust, is close to the western cluster, and one of its nodal planes is oriented NW, as the cluster, and dips to the

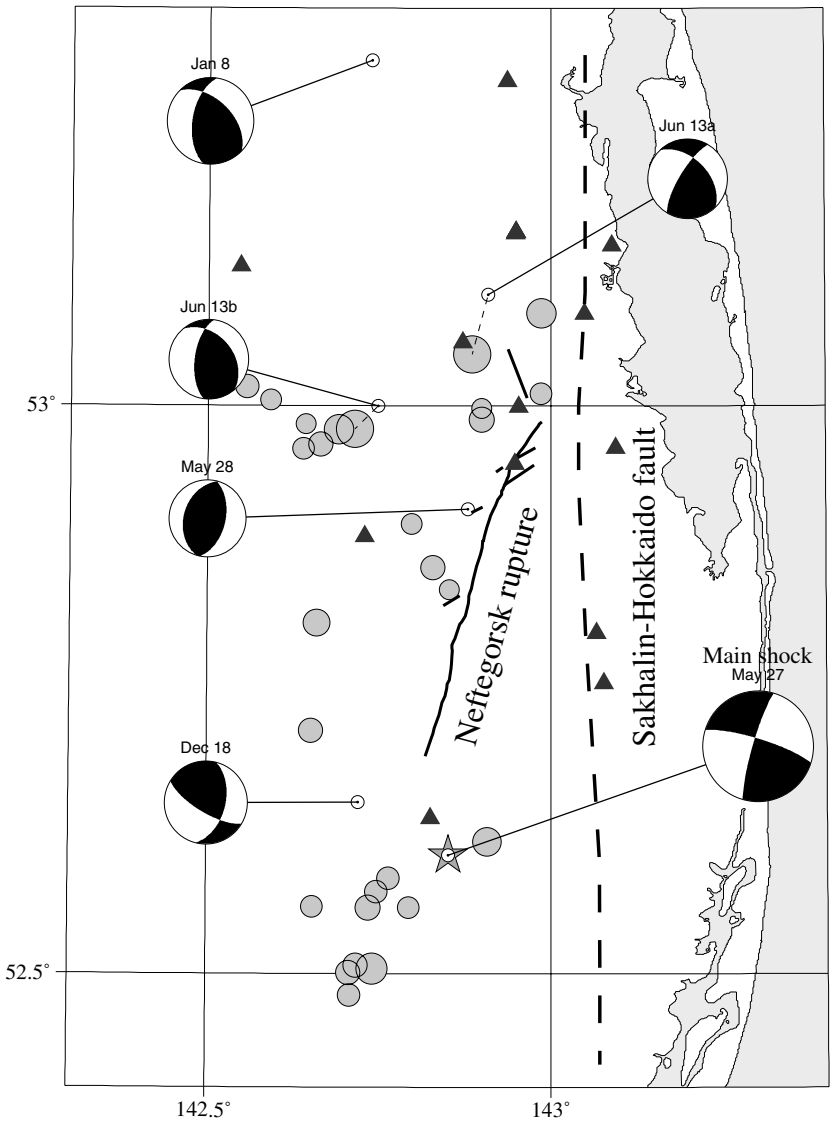

Figure 7. Strongest aftershocks (3.6 < Magnitude < 5.0), surface ruptures and available Harvard CMT solutions for aftershocks. Triangles are temporary seismic stations. Shaded circles are epicentres from the local network. Open circles are NEIC locations. The star is the NEIC epicentre of the main shock.

NE. The January 8 aftershock (more than six months after the main shock) has a mechanism that is close to those of June 13, but it is far from the aftershock cloud and is not easily related to surface ruptures of the main shock. The aftershock of December 18 (about half a year after the main shock) is located close to the Piltoun fault, with a mechanism which is roughly consistent with the motion along this fault.

BODY WAVE INVERSION

Body waveform inversion has been applied to a selected set of broad-band global network records (GDSN) in order to obtain a kinematic model of the source (Nabelek 1984). We used the standard version of the IASPEI software (McCaffrey & Abers 1988). In general, many model parameters can be adjusted, and the requirement of a best fit between observed and calculated wave forms can lead to physically unrealistic results due to trade-offs. In the case of the Neftegorsk earthquake, however, the rupture reached the surface, and it was precisely mapped with the help of GPS positioning. Furthermore, the geometry of the aftershock cloud was also well resolved thanks to epicentral observations obtained with a local network. This independent information helped us to reduce the uncertainty in modelling the source.

Digital records ($30^\circ < \Delta < 90^\circ$) were deconvolved by the individual instrumental responses, and then convolved with

a common broad-band instrument, for easy comparison of neighbouring records. We used channels LH and BH. All of the records were sampled again at a uniform time interval of 0.5 s for *P* waves (BH channel only) and 1.0 s for *S* waves (*SH* components only). Zero line correction, linear trend, taper, and correction of initial points were applied during the integration procedure (velocity to displacement). We also compared shapes and amplitudes of waves on neighbouring stations, which should be similar except for nodal ones. A few noisy stations were eliminated, and the final data set is shown in Fig. 8.

Azimuthal coverage around the source was not homogeneous: the Pacific Ocean (with a few stations on islands), the eastern part of Russia and China are areas with insufficient data, while the territory of USA and Europe, including western Russia (where the number of stations is comparably large) are well covered. Most of the available records correspond to epicentral distances between 55° and 85°, and some to the interval $30^\circ - 50^\circ$.

Following Nabelek (1984), the inversion of the focal mechanisms and the far-field source-time function were obtained by minimizing the sum of the square of residuals between observed and calculated signals. The inverted parameters comprise the double-couple mechanism (strike, dip and rake), the scalar seismic moment, the depth, the source-time function, the relative spatial location (in our case the location was fixed from knowledge of the surface rupture) and the time delays for each source. The relationship between the model and the source parameters is non-linear, so minimization was achieved by an iterative procedure, with linearization at each step. Anelastic attenuation along the ray path was also taken into account through the operator t^*, with a commonly used value of $t^* = 0.7$ s for *P* waves and $t^* = 4.0$ s for *SH* waves (Futterman 1962). For the inversion procedure we used a weight of 0.3 for *SH* waves due to their smoother character and larger amplitude relative to *P* waves. We simplified the velocity model used for epicentral determinations (Arefiev *et al*. 1995), and selected a two-layer model (Table 1b).

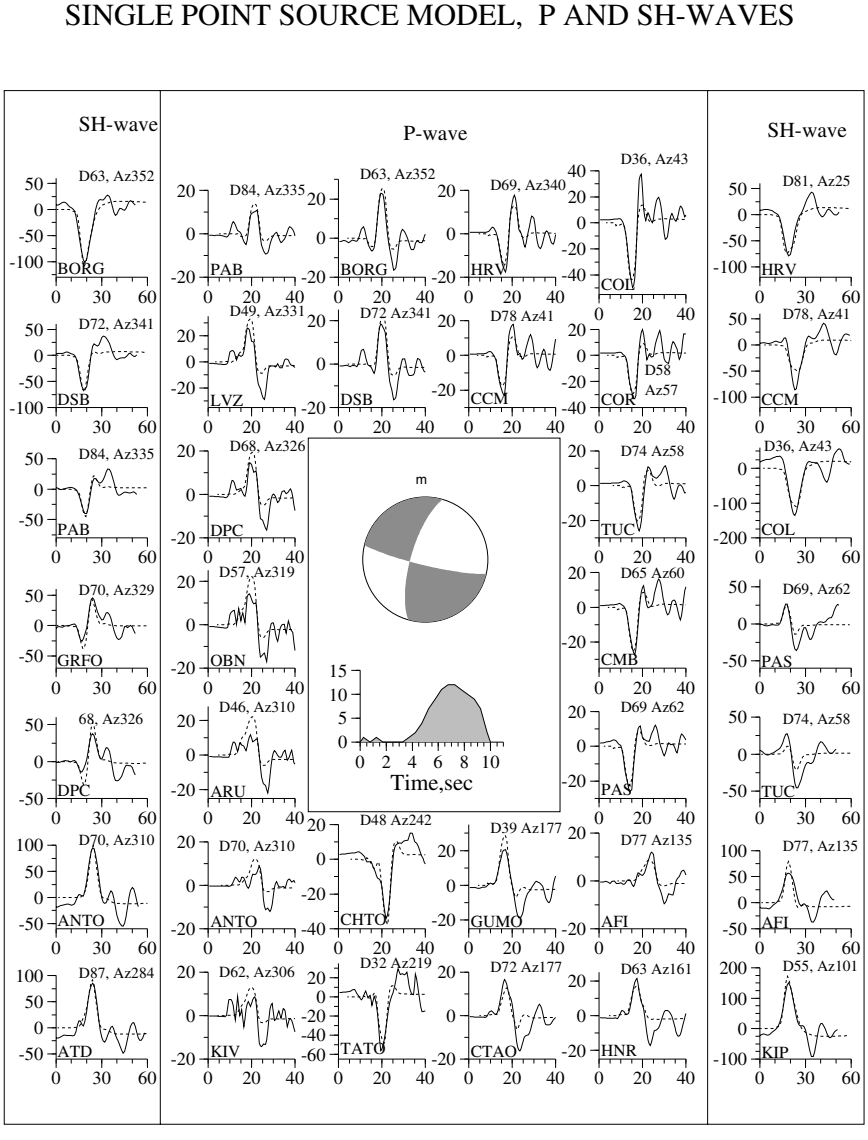

Figure 8. Focal mechanism from the inversion for a single point source. *P*- and *SH*-wave displacements (microns) are shown. Solid lines are observed signals and dashed lines are calculated ones. The azimuthal distribution of stations can be found in Table 4. The moment rate output (centre) has a shape close to a triangle. The initial *P* pulse at stations OBN, DSB, HNR and others is not explained by this model.

Step 1: As a first step we modelled the source as a single point source located at the epicentre. The results are presented in Fig. 8. The calculated seismograms fit the observed waveforms fairly well. The source parameters we obtained are given in Table 2. The single-source time function had a simple shape too, as shown in Fig. 8, and it can be approximately parametrized by one triangle. The two solutions, our mechanism and the Harvard CMT solution, are in good agreement. The moment obtained by the CMT solution is slightly larger, but the centroid depth of 23.6 km used by the CMT is doubtful for a surface rupture with aftershocks shallower than 15 km (depths are well controlled by the local network).

The point-source focal mechanism given by the Harvard CMT solution and our simple model fit the observations fairly well. However, a number of features cannot be explained by such simple solutions:

(1) some aftershock clusters make an angle with respect to the orientation of the main surface rupture and suggest hidden branches;

(2) the surface breaks observed at the northern end of the rupture zone are oriented NNW;

(3) the CMT inversion shows a significant non-double-couple component (15 per cent of the total moment);

(4) the waveform data from the worldwide network show an initial pulse at the beginning of the *P* phase on a number of stations mainly to the northwest of the source.

It is impossible to model such an impulse with a source having the same simple geometry as the main rupture, even using a complex time variation, and hence we need to add subsources having a different orientation.

The distribution of stations as a function of azimuth is not homogeneous. Therefore, in order to investigate the effects of the direction of the source propagation and rupture velocity (directivity), we decided not to rely on azimuthal weighting since it is difficult to control this process correctly. Instead, we selected a subset of 11 typical stations with an almost homogeneous distribution in azimuth. In order to check our selection, we used signals only from these stations and inverted for a simple point source, obtaining practically the same result as above.

The main fault plane, as inferred from surface ruptures and the aftershock distribution, is oriented nearly N–S and dips about 70° westwards. There are two possibilities for unilateral rupture propagation: southwards or northwards. We investigated them by computing several inversions for different values and orientations of the rupture velocity, while keeping fixed the strike and the dip, which were well controlled in the field. The best results are obtained for a rupture direction, across the fault plane, varying from N20° to N90°, and a rupture velocity of between 1.5 and 3.0 km s^{-1}. These are indeed very general constraints.

Table 2. Fault mechanism, depth, and moment for a single-source model.

Agency	Strike	Dip	Rake	Depth (km)	M_0 (dyn cm)
CMT (Harvard)	196	82	169	23.6	4.32×10^{26}
Our determination	196	71	188	6.7	3.23×10^{26}

Next, we retained the point source and simplified the source-time history, modelling it as one triangle. The relative rms error versus rise time τ was calculated, giving a well-defined minimum error at $\tau = 3.6$ s and a total source duration of 7.2 s.

We then assumed a rupture propagating from south to north, and searched for a reasonable rupture propagation velocity. Given that the total rupture length at the surface is not less than 40 km and that the source duration is not more (the essential part of moment release) than 7 s, we found that we had an unrealistic rupture velocity of about 6 km s^{-1} for a unilateral rupture propagation. This high value led us to explore the case of bilateral rupture propagation, as shown below.

Step 2: Segmentation and branching is a common feature observed in large earthquakes, the aftershocks clustering around the broken segments (see Dorbath *et al*. 1992, for instance). In the case of Neftegorsk, a local minimum on the horizontal component, together with a change in sign of the vertical component, can be distinguished at a latitude of 52.83°N (see Fig. 4). Hence we propose two segments (II and III, Fig. 10) of roughly equal length for the main rupture.

Moreover, Figs 5 and 6 show a dense cluster west of the main aftershock cloud, and of the main surface rupture. We suggest that it may be associated with a NW-trending blind fault (I in Fig. 10) generated during the main shock. Segment (2) in Fig. 3(b) illustrates the existence of such faults at the surface. This hidden branch would pass through the boundary between segments II and III, which would then become a triple point. It is unlikely that such a segment could be broken after the main shock, since there were no strong aftershocks there ($M \geq 4$) during the first two weeks. These considerations, together with the presence of an impulse at the beginning of the *P* wave group at some stations located NW and SE of the source, and the absence of such an impulse at stations at other azimuths (Fig. 8), led us to propose such a NW-oriented branch as the first segment of the rupture.

Finally, a fourth NW-oriented segment (IV in Fig. 10) at the northern end of the rupture zone can be observed at the surface, though not continuously (Rogozhin 1995 and Fig. 4), and at depth as an aftershock cluster.

These subsources would break in the following order: the rupture starts at the western subsource (I), as shown by the impulses on records at northwestern azimuths. Then, the southern (II) and northern (III) segments of the fault rupture almost simultaneously, and finally the process ends at the northernmost segment (IV), which is oriented NW. In fact, some effect of rupture propagation from south to north was revealed (between N20° and N90°) when modelling the source by a simple rupture. Furthermore, it should be noted that the PDE epicentre location in the southern part of the rupture, although not very accurate in this region, provides indirect evidence for some amount of south–north propagation.

When modelling the complex source of the Neftegorsk earthquake we fixed the following parameters: (1) the strike of all subsources; (2) the order of rupture of the four subsources. All other parameters of the complex source (dip, rake, moment, duration) were determined for each subsource by the inversion procedure. The result of this inversion is shown in Table 3 and Figs 9 and 10, and gives the best fit for this geometry. The total seismic moment is $M_0 = 4.24 \times 10^{26}$ dyn cm, very similar to that of the Harvard solution.

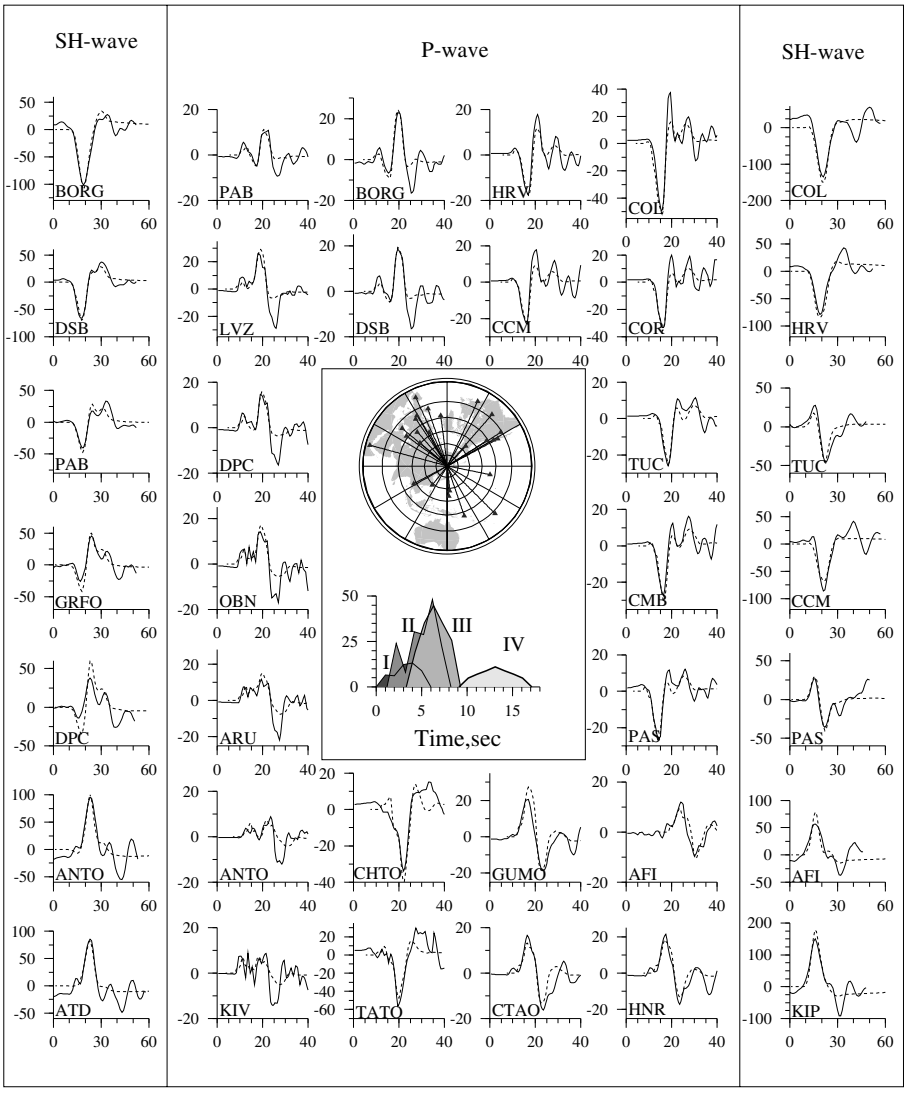

Figure 9. Inversion result for a complex source. Displacement amplitude (microns) is shown as a function of time (s). The seismic moment rate output for the four subsources is shown at the centre, with the vertical scale in units of 10^{24} dyn cm s^{-1}. The rupture initiates at subsource I, near the middle of the observed surface breaks, and propagates bilaterally along subsources II and III. This model (Fig. 10) provides the lowest rms error.

We also checked some other possible solutions. First, we considered the fact that the orientation of the northernmost segment is NW, so that in principle it could also produce the pulse at the beginning of *P* waves observed at NW and SE azimuths. A check was done for the subsources in the order IV–III–II, and excluding the western subsource I. It was not, however, possible to achieve good agreement between synthetic and observed records for this case.

We could find an even better fit between synthetics and data for the order of the subsources that was accepted during the inversion (sequence I–II–III–IV) if we did not fix the NW orientation of subsource number IV (which corresponds to the orientation of the surface rupture at this place). In this case, the dip and strike of subevent IV become similar to those of subevents II and III, but its rake is in contradiction to the regional stress tensor.

Table 3. Complex source parameters.

Subsource	Strike	Dip	Rake	Depth (km)	$M_0 \times 10^{25}$	dT (s)	X	Az
I	156	41	116	8.0	4.7	–	–	–
II	191	75	208	5.4	16.0	1.2	18	169
III	202	62	168	7.8	16.1	3.3	8	75
IV	160	77	319	12.4	5.3	9.1	16	38

DISCUSSION AND CONCLUSIONS

The Neftegorsk earthquake was unexpected, since it was not associated with the main tectonic structure of the region (the Sakhalin–Hokkaido strike-slip fault) but with the secondary

Table 4. Azimuth and distance of stations used in the body waveform inversion.

N	Station	Delta (°)	Azimuth (°)
1	HRV	80.8	25.1
2	CCM	78.3	40.8
3	COL	36.1	42.6
4	COR	58.3	56.9
5	TUC	74.0	57.7
6	CMB	64.6	60.3
7	PAS	68.7	61.6
8	KIP	54.5	101.1
9	AFI	76.8	134.8
10	HNR	63.4	161.1
11	CTAO	72.3	176.7
12	GUMO	38.8	176.9
13	TATO	31.9	218.8
14	CHTO	47.9	242.4
15	ATD	87.0	284.9
16	KIV	62.0	306.4
17	ANTO	69.9	309.7
18	ARU	46.3	310.1
19	OBN	56.7	318.7
20	DPC	68.0	326.3
21	GRFO	70.3	329.0
22	LVZ	48.7	331.4
23	PAB	84.0	335.1
24	DSB	68.9	340.0
25	BORG	62.5	352.4

NEFTEGORSK EARTHQUAKE FINAL SOURCE MODEL

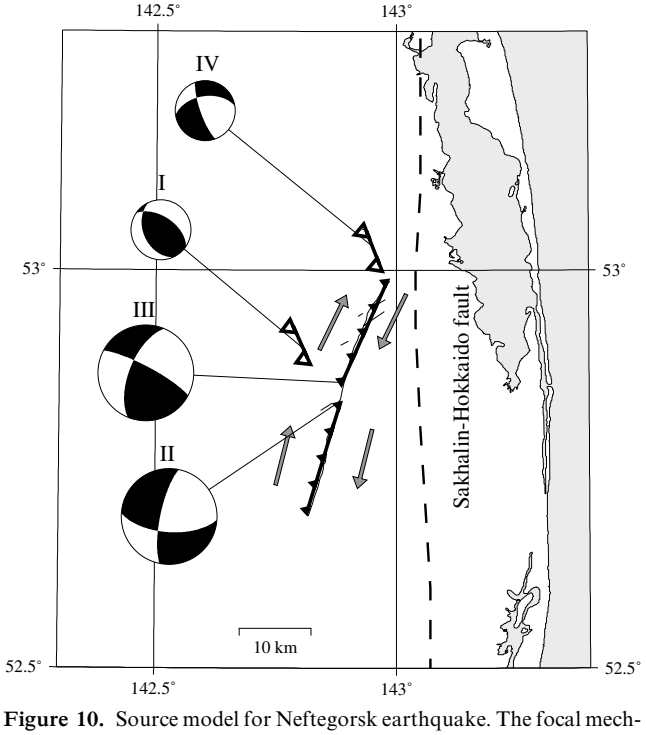

Figure 10. Source model for Neftegorsk earthquake. The focal mechanism of each subsource is shown, together with their time sequence and their location. Surfaces ruptures and sense of displacement are shown for comparison.

Upper Piltoun fault, breaking it along practically its entire length. This secondary fault connects the Sakhalin–Hokkaido and the Middle Sakhalin faults. The very large slip observed at the surface (up to 8 m) is quite unusual for a magnitude $M_S = 7.6$ earthquake. The low level of seismic activity observed in the vicinity of the Upper Piltoun fault before the earthquake (although the known history is less than 100 years) suggests the accumulation of strain for a long time on some locked segments. The strongest aftershock had magnitude M_S less than 5. The absence of strong aftershocks might indicate that the strain, accumulated over a long time, was almost totally released during the main shock, in accordance with the unusually large slip value.

We estimated the principal parameters of the Neftegorsk earthquake source by using only data from the epicentral area. From the aftershock cloud geometry we were able to evaluate the down-dip width to be between 10 and 15 km (Fig. 6). The maximum value of rupture length obtained from the aftershock cloud is between 60 and 70 km. However, it should be remembered that epicentral observations started two weeks after the main shock, so no high-quality locations are available for early aftershocks. Moreover, the region affected by aftershocks grows with time, and thus provides only an upper bound for the rupture surface of the main shock. The surface rupture length, on the other hand, was precisely measured at the surface (Fig. 4). The minimum estimation for the rupture length is 40 km, not including the NW-oriented surface rupture for the main earthquake, under the hypothesis that it appeared as the result of a strong aftershock. There were only three strong aftershocks during the first month (May 28, $M_S = 4.7$; June 13, $M_S = 4.5$; June 13, $M_S = 4.8$). The two last events were registered by the local network, and only one of them was located on the northwestern branch. The corresponding ruptures are about 1 km long (Wells & Coppersmith 1984), while the observed surface rupture is five times longer. Hence, this branch was probably activated by the main shock, giving a total rupture length of 46 km.

The Neftegorsk earthquake can be described, in the first approximation, as a simple point source. In order to explain several particular features, however, it was necessary to use a more complex source model. One of the elements contributing to the complex source is segment I in Fig. 10. This orientation corresponds to the western aftershock cluster, and can be seen in satellite images but not in the geological map, nor among the surface ruptures. This segment seems to be the place where the whole complex rupture process started.

We propose the following scenario for the rupture process of the Neftegorsk earthquake, taking into account all available data. The event started with a relatively short rupture (11 per cent of the total seismic moment), located west of the centre of the main fault. After 1.2 s, bilateral rupture propagation began along the main fault, first towards the south (with 38 per cent of the total moment), and then towards the north (38 per cent of the total moment and with a delay of 2.1 s). Finally, the last segment, oriented NW, broke at the northern end of the main fault (13 per cent of the total moment), some 5.8 s after the previous one. The total time duration of the main part of the source was short because bilateral rupture propagation permits subevents to overlap in time.

Average values of 46 km for the length of the surface rupture, and 12 km for the width of the aftershock cloud may be used with an average slip of 3.9 m at the surface, or

with 5.2 m if we consider the value obtained from geodetic measurements by Takahasi *et al*. (1995). Therefore the near-field seismic moment varies between 6.5×10^{26} and 8.6×10^{26}, as compared with 4.3×10^{26} obtained from body wave modelling and the Harvard surface wave modelling.

The right-lateral strike-slip motion during the Neftegorsk earthquake is in agreement with plate tectonics in this region. However, the main rupture took place along a secondary fault, the Piltoun fault, which has a rather complex geometry.

ACKNOWLEDGMENTS

We are grateful to all participants of the Epicentral Expedition who collected and processed data from observations, and especially to Dr A. Kozhurin for geological data. Most drawings were made using the GMT free software. This work was supported by the Russian Foundation for Basic Research, project no. 99–05–65418. We thank S. Goes and an anonymous reviewer for their careful reading of the manuscript and their numerous helpful observations.

REFERENCES

Arefiev, S. *et al.*, 1995. The preliminary results of epicentral observations the Neftegorsk earthquake May 27 (28), 1995, *Information Analysis Bulletin FSSN, special issue, Moscow,* pp. 36–47 (in Russian).

DeMets, C., Gordon, R.G., Argus, D.F. & Stein, S., 1990. Current plate motions, *Geophys. J. Int.,* **101,** 425–478.

Dorbath, L., Dorbath, C., Rivera, L., Fuenzalida, L., Cisternas, A., Arefiev, S., Tatevossian, R. & Aptekman, J., 1992. Geometry, segmentation and stress regime of the Spitak (Armenia) earthquake from the analysis of the aftershock sequence, *Geophys. J. Int.,* **108,** 309–328.

Futterman, W.I., 1962. Dispersive body waves, *J. geophys. Res.,* **67,** 5279–5291.

Ivashenko, A. *et al.*, 1995. The Neftegorsk earthquake May 27, 1995 on Sakhalin, *Information Analysis Bulletin FSSN, special issue, Moscow,* pp. 48–67 (in Russian).

Kharakhinov, V., Galtcev-Bezuk, S. & Tereshcenkov, A., 1984. The faults of Sakhalin, *Tikhookeanskaya geologia,* **2,** 77–86 (in Russian).

Kozhurin, A. & Streltsov, M., 1995. Seismotectonical manifestation the North Sakhalin earthquake of May 27 (28), 1995, *Information Analysis Bulletin FSSN, special issue, Moscow,* pp. 95–100 (in Russian).

Lee, W.H.K. & Lahr, J.C., 1975. HYPO71 (revised): a computer program for determining hypocenter, magnitude and first motion pattern of local earthquakes, *USGS, Open File Report 75–311.*

McCaffrey, R. & Abers, G., 1988. SYN3: a program for inversion of teleseismic body waves forms on microcomputers, *Air Force Geophysical Laboratory Technical Report, AFGL-TR-88–0099,* Hanson Air Force Base, MA.

Nabelek, J., 1984. Determination of earthquake source parameters from inversion of body waves, *PhD thesis,* MIT, Cambridge, MA.

Oskorbin, L., Poplavskii, A. & Zanuikov, V., 1967. The Noglik earthquake of October 2, 1964, Yuzhno-Sakhalinsk (in Russian).

Rogozhin, E., 1995. The Neftegorsk earthquake May 27, 1995: geological evidence and tectonic setting, *Information Analysis Bulletin FSSN, special issue, Moscow,* pp. 80–94 (in Russian).

Rogozhin, E., 1996. The tectonic of source zone Neftegorsk May 27, 1995 earthquake on Sakhalin, *Geotektonika,* **2,** 45–53 (in Russian).

Rozhdestvenskiy, V., 1975. The strike-slips of North Sakhalin, *Geotektonika,* **2,** 85–97 (in Russian).

Semenov, R., Kharakhinov, V. & Pavlenov, A., 1996. The large North Sakhalin Earthquake of May 28, 1995: a seismogeological description, *Izvestiya, Phys. solid Earth,* **32,** 1032–1036.

Shimamoto, T., Watanabe, M. & Suzuki, Y., 1995a. The Neftegorsk earthquake surface rupture, *Information Analysis Bulletin FSSN, special issue, Moscow,* pp. 101–116 (in Russian).

Shimamoto, T., Watanabe, M., Suzuki, Y., Kozhurin, A.I., Strelizhov, M.I. & Rogozhin, E.A., 1995b. Surface faults associated with Neftegorsk earthquake, *J. Geol. Soc. Japan,* **101.**

Strakhov, V.N., 1995. The Neftegorsk earthquake 27(28).05.1995. *Information Analysis Bulletin FSSN, special issue, Moscow* (in Russian).

Takahasi, Kh., Vasilenko, N., Kimata, F., Kasahara, M., Seno, T., Kim, Ch.U. & Ivashenko, A., 1995. Coseismic deformation in the northern part of the epicentral zone of the 1995 Neftegorsk earthquake from geodetic observations, *Information Analysis Bulletin FSSN, special issue, Moscow,* pp. 80–94 (in Russian).

Wells, D. & Coppersmith, K., 1984. New empirical relationships among magnitude, rupture length, rupture width, rupture area, and surface displacement, *Bull. seism. Soc. Am.*, **84,** 974–1002.